Geomechanics and Engineering, Vol. 3, No. 4 (2011) 291-321
DOI: http://dx.doi.org/10.12989/gae.2011.3.4.291

Comparison of numerical and analytical solutions for reinforced soil wall shaking table tests

Saman Zarnani[1], Magdi M. El-Emam[2] and Richard J. Bathurst*[3]

[1]*BGC Engineering, Vancouver, British Columbia, Canada*
[2]*Department of Civil Engineering, College of Engineering, American University of Sharjah, Sharjah, United Arab Emirates*
[3]*GeoEngineering Centre at Queen's-RMC, Department of Civil Engineering, Royal Military College of Canada, Kingston, Ontario, Canada*

(Received February 19, 2011, Revised November 14, 2011, Accepted November 16, 2011)

Abstract. The paper describes a simple numerical FLAC model that was developed to simulate the dynamic response of two instrumented reduced-scale model reinforced soil walls constructed on a 1-g shaking table. The models were 1 m high by 1.4 m wide by 2.4 m long and were constructed with a uniform size sand backfill, a polymeric geogrid reinforcement material with appropriately scaled stiffness, and a structural full-height rigid panel facing. The wall toe was constructed to simulate a perfectly hinged toe (i.e. toe allowed to rotate only) in one model and an idealized sliding toe (i.e. toe allowed to rotate and slide horizontally) in the other. Physical and numerical models were subjected to the same stepped amplitude sinusoidal base acceleration record. The material properties of the component materials (e.g. backfill and reinforcement) were determined from independent laboratory testing (reinforcement) and by back-fitting results of a numerical FLAC model for direct shear box testing to the corresponding physical test results. A simple elastic-plastic model with Mohr-Coulomb failure criterion for the sand was judged to give satisfactory agreement with measured wall results. The numerical results are also compared to closed-form solutions for reinforcement loads. In most cases predicted and closed-form solutions fall within the accuracy of measured loads based on ± 1 standard deviation applied to physical measurements. The paper summarizes important lessons learned and implications to the seismic design and performance of geosynthetic reinforced soil walls.

Keywords: reinforced soil walls; seismic; shaking table; numerical modelling; FLAC.

1. Introduction

Geosynthetic reinforced soil (GRS) retaining walls are now a mature technology since their introduction in the late 1970s (Allen *et al*. 2002). Design and analysis methods for walls in static load environments are also well-established and the accuracy of internal stability design methods for these structures has been assessed through comparison with full-scale instrumented structures (e.g. Allen *et al*. 2003, Bathurst *et al*. 2008). There is also a growing body of literature that shows GRS walls have behaved well during earthquake compared to conventional soil retaining walls. A

*Corresponding author, Professor, Research Director, Ph.D., E-mail: bathurst-r@rmc.ca

description of some of these structures can be found in the case studies noted by Bathurst *et al*. (2002) and Koseki *et al*. (2008). Nevertheless, the development of analytical and numerical methods to predict the behaviour of GRS walls under seismic loading lags that for static loading conditions. This situation is largely due to the practical difficulty of monitoring full-scale structures subjected to earthquake and the complexity of the mechanical interactions between wall components under dynamic loading conditions. A strategy to improve our understanding of the response of GRS walls to earthquake is to carry out numerical simulations using numerical models that have been verified against physical models constructed on a centrifuge or 1-g shaking tables.

This paper first provides a review of related work in which numerical model results of GRS walls under simulated earthquake loading have been compared to the results of physical tests using centrifuge or 1-g shaking tables. The major focus of the paper is on the development of a FLAC numerical model for two 1-g reduced-scale model shaking table tests previously reported by the writers that were constructed with very different boundary conditions (i.e. hinged toe and sliding toe conditions). Simulation results using this model are compared to a wide range of physical measurements. Numerically predicted and measured reinforcement loads are then compared to values using three different pseudo-static closed-form solutions found in the literature and in current North American design guidance documents. The paper concludes with lessons learned and some implications of numerical, closed-form and physical test results to the internal stability design and performance of geosynthetic reinforced soil walls subject to earthquake loading.

2. Previous related work

Previous related work on numerical modelling of the seismic response of geosynthetic reinforced soil (GRS) walls can be divided into different categories: a) parametric investigations using programs that were not verified against physical tests, and; b) numerical parametric investigations that were based on numerical simulations verified against results of centrifuge shaking table tests, full-scale 1-g shaking table tests and reduced-scale 1-g shaking table tests. This partition is useful since the value of previous numerical simulation studies is influenced by whether or not the accuracy of numerical models was investigated by comparison with physical test results and the type of physical tests that were used in the comparison.

There are a large number of studies that fall into the first category. For brevity these studies are not reviewed in this paper. Nevertheless, later in the paper reference is made to some of these studies which were used to guide numerical modelling in the current investigation or to corroborate lessons learned. Examples of useful unverified numerical investigations are the work reported by Cai and Bathurst (1995), Bathurst and Hatami (1998), Hatami and Bathurst (2000, 2001), Hatami *et al*. (2005), Vieira *et al*. (2006).

2.1 Centrifuge shaking table tests

Ling *et al*. (2004) used a nonlinear dynamic finite element model (FEM) program to simulate the dynamic behaviour of five 0.15-m high reinforced soil wall models mounted on a centrifuge shaking table. The sandy backfill soil was modelled with a 15-parameter generalized plasticity model which was able to simulate pressure-dependent stress-strain-dilatancy behaviour of the backfill. The uniaxial cyclic behaviour of the geogrid layers was modelled with a nine-parameter

bounding surface model. The numerical analyses were conducted using the dimensions of the centrifuge models but the results transformed to prototype scale. They compared acceleration response in the backfill, wall facing movement and backfill surface settlement between the numerical and experimental results and concluded that the numerical procedure was able to simulate the dynamic behaviour of the model walls; however, the validity of centrifuge model results transformed to full-scale structures could not be guaranteed. Ling *et al*. (2005a) used the same dynamic FEM program to conduct a numerical parametric study on the static and seismic behaviour of 6-m high modular block GRS retaining walls constructed on a 3-m thick soil foundation. The parameters investigated in this study were: the dilatancy and cyclic hardening behaviour of the backfill soil, the weight of the concrete blocks used to construct the facing, interface friction angle between the blocks and the backfill, the vertical spacing and length of the reinforcement layers and earthquake motions as input excitation of numerical models (with non-matching peak acceleration magnitudes and predominant frequencies). They concluded that the lateral displacement of the wall and the wall crest settlement were influenced by soil cyclic behaviour, reinforcement layout and earthquake motion characteristics. The loads in the reinforcement layers were influenced by the earthquake record and vertical spacing of reinforcement layers. Amplification of acceleration was affected by the soil behaviour and earthquake record but not by the reinforcement layout. The effects of reinforcement vertical spacing were more significant compared to the length of the reinforcement.

Fujii *et al*. (2006) used a FEM numerical code to simulate the dynamic response of 13 variations (cases) of a 0.15 m-high GRS wall tested in a 50 g centrifuge. The variables were the type of input excitation, frequency and amplitude. The numerical model was developed to simulate prototype scale (i.e. 7.5-m high wall). The calculated and measured values of acceleration response, wall displacement and horizontal earth pressure behind the wall were compared. They concluded that the maximum response acceleration for all cases calculated by the numerical analysis was about 10-20% larger than the values measured in the tests. Lateral wall displacements were judged to be in good agreement. However, the predicted maximum horizontal earth pressures behind the wall were up to 400% larger than measured values. They suggested that this discrepancy may be attributed to the choice of interface model between the wall facing and backfill soil.

While centrifuge testing of complex reinforced soil structures can provide useful qualitative insights regarding system response, their use is problematic if the objective is accurate quantitative predictions of structure response at prototype scale. For example, in the work by Ling *et al*. (2004), the 0.2-mm thick model reinforcement layer at 50 g becomes 10 mm at prototype scale which is not reasonable. If wall performance at failure is an objective, then the influence of sand particle size on shear band behaviour is also an issue (Tatsuoka *et al*. 2010).

2.2 One-g shaking table tests

Helwany *et al*. (2001) used the finite element method program DYNA3D (Hallquist and Whirley 1989) to simulate the experimental results of a shaking table test on a 0.9-m stack of segmental (modular) blocks reinforced with five geotextile layers. While all components in the physical test were prototype-scale, the stack was very short and not typical of these structures in the field. They used a hysteretic energy dissipating model (Ramberg-Osgood model) to simulate the sandy backfill. They compared the measured and calculated wall response (wall displacement and acceleration response) at 0.5 g base acceleration and concluded that there was close agreement between the

numerical and experimental results. Helwany and McCallen (2001) used the verified numerical model to investigate the effects of wall facing details on the seismic behaviour of a 6-m high segmental reinforced retaining wall subjected to a recorded earthquake loading (El Centro 1940), including nonlinear contacts between various wall components and nonlinear hysteretic energy dissipation soil behaviour. The writers concluded that the predicted small earthquake-induced lateral facing deformations, connection loads, and axial strains in the geosynthetic layers suggest that the retaining wall in their study would not experience any significant distress if subjected to the El Centro earthquake.

Lee *et al*. (2010) used the finite element method program LS-DYNA to numerically simulate the dynamic performance of three of four large-scale shaking table walls reported by Ling *et al*. (2005b). The sand soil in these simulations was modelled by a cap model which required more than 10 parameters. However, hysteretic behaviour and soil dilatancy is not captured in this model. The geogrid layers were modelled with shell elements having a plastic-kinematic model which required four parameters. Different response values from numerical simulations were compared against physical measurements such as: lateral earth pressure, wall displacement, bearing pressure, reinforcement tensile load, backfill settlement and acceleration response. However, because there are no estimates of the accuracy of physical measurements, Lee *et al*. (2010) concluded that the predictive accuracy of their numerical model required further investigation.

Ling *et al*. (2010) used the results of four large-scale shaking table walls reported by Ling *et al*. (2005b) to verify their numerical models developed with a small-deformation, nonlinear dynamic finite element procedure (DIANA-SWANDYNE-II, Chan 1993). The sand was modelled with a uniform generalized plasticity model based on the concept of critical state which requires 16 parameters. The geogrid was modelled using a one-dimensional bounding surface concept described by 10 parameters. The selection of Rayleigh damping coefficients for the soil was investigated by Ling *et al*. (2010) who determined that for models with a peak acceleration of 0.4 g, a 15% damping value produced the most satisfactory results. For models with maximum acceleration of 0.8 g, the damping was lowered to 5%. Predicted wall deformations, backfill settlement, reinforcement loads and acceleration response were compared to measured values. They concluded that the time response of wall accelerations at different locations in the walls was satisfactory but not deformations. Tensile loads in the reinforcement were slightly over-estimated. They also acknowledged that the effect of Rayleigh damping on the response of numerical models required further investigation.

2.3 Remarks

The large-scale 1-g physical models reported by Ling *et al*. (2005b) are the best candidates for numerical modelling verification currently available in the literature. Nevertheless, despite complex constitutive models for the component materials the accuracy of predictions was not always satisfactory (Ling *et al*. 2010, Lee *et al*. 2010). Another important factor not discussed in these physical tests is the truncated soil volume extending behind the facing units (i.e. B/H = 1.3 where B is the toe to far-field boundary and H is the height of structure). Inertial effects during shaking can be expected to increase with size of retained soil volume as demonstrated in parametric analyses reported by Bathurst and Hatami (1998). The advantage of the reduced-scale 1-g tests used in the current study is that the ratio of B/H = 2.4 which is demonstrated to be sufficient to contain the disturbed zone of soil in both physical and numerical models. Not available in the papers by Ling *et al*. (2005a, 2005b) are any estimates of the accuracy of physical measurements of reinforcement

load. As demonstrated in the current study, qualitative assessments of the accuracy of any numerical model should be influenced by the spread in physical measurements. Stated alternatively, the accuracy of a numerical model need only be as accurate as the physical measurements against which comparisons are made. Nevertheless, 1-g shaking table model tests of the type described in this paper are carried out under confining stress levels that are lower than prototype scale. Hence, the response of stress-dependent soils may be different between model and field-scale structures and thus quantitative and qualitative projections of model behaviour to field scale must be made with caution. Despite this shortcoming, parametric numerical studies using numerical models verified against results of reduced-scale shaking table tests are the most practical strategy available today to develop an understanding of retaining wall behaviour due to earthquake (Wood *et al*. 2002).

3. Current study

This paper describes the development of a numerical model using FLAC (Itasca 2005) and its verification against quantitative measurements from two well-instrumented 1/6-scale models tested on a large 1-g shaking table (El-Emam and Bathurst 2004, 2005). This paper is an expanded version of two earlier conference papers (El-Emam *et al*. 2001, 2004). The two physical tests described in this paper are from a series of 14 model tests carried out at RMC (wall models 7 and 8) (El-Emam 2003). This paper briefly describes: a) the two physical test model walls that varied only with respect to toe boundary condition; b) numerical approach, and; c) material constitutive models adopted and the selection of model parameters from independent laboratory tests. Numerical results are compared to measured facing panel lateral displacements, reinforcement loads, horizontal and vertical toe loads, and accelerations at different locations. A third physical test (wall model 1) is introduced later in the paper to compare observed and numerically-predicted soil shear zones developed in the backfill at the end of base excitation.

In previous related work by other researchers, constitutive models of widely varying complexity were used for the component materials. An important feature of the current study is that simple linear elastic-plastic models with M-C failure criterion were judged to give satisfactory predictions. Previous related studies have compared numerical predictions to wall displacements, reinforcement strains, foundation pressures and accelerations. A unique feature of the current study is that numerical predictions are also compared to vertical and horizontal boundary toe loads. This is not only an important check on the accuracy of numerical results but also highlights the importance of wall toe compliance on wall response under both static and dynamic loading conditions. Finally, the current study also compares numerical simulation predictions of reinforcement loads and measured values to closed-form (analytical) solutions found in the literature and in North American design guidance documents.

4. Physical wall models

A schematic cross section of the 1/6-scale model walls including instrumentation is shown in Fig. 1. For brevity only a brief description of the physical test arrangement is reported here. Details are reported by El-Emam (2003) and El-Emam and Bathurst (2004).

The reinforcement vertical spacing was S_v = 0.225 m and the reinforcement length to height ratio

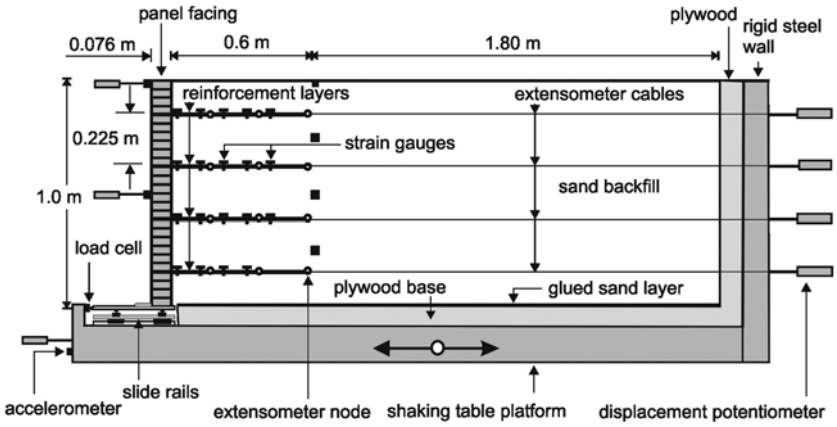

Fig. 1 Schematic diagram of 1/6-scale shaking table model wall and instrumentation

was L/H = 0.6. Similitude rules proposed by Iai (1989) were used so that geosynthetic reinforcement stiffness satisfied a model to prototype scale ratio of 1/6. The two models were nominally identical structures except for the toe boundary. In one model wall (hinged toe), the toe was restrained from relative movement (i.e. relative to the shaking table) in the vertical and horizontal directions, while it was free to rotate. In the companion model wall (sliding toe), the toe was free to slide horizontally and rotate, but was restrained from vertical movement. It can be argued that field walls fall between these two idealized conditions because field walls are typically constructed with toe embedment and a footing that provide some horizontal compliance (Huang *et al*. 2010).

In each model wall, the wall facing panel consisted of a column of rectangular hollow steel sections bolted together to form a 1-m high rigid facing with a thickness of 76 mm and a width of 1.4 m. The reinforcement connections with the facing panel were designed to be perfectly rigid to prevent slippage of the reinforcement layers at the facing and thereby simplify the interpretation of results. The friction between the backfill soil and sides of the test box was minimized by placing a composite arrangement of Plexiglas and lubricated polyethylene sheets over the sidewalls.

The backfill was poorly graded sand with angular to sub-angular particles (maximum particle size = 2 mm) resulting in high friction angle. The coefficient of curvature and uniformity are 1.27 and 2.5, respectively. This material is a commercial sand-blasting material and was purposely selected because it is silica-free and therefore satisfied health and safety regulations for indoor laboratory environments. The sand was placed dry and gently vibro-compacted (using the shaking table) in 100-mm lifts to a relative maximum dry density of 86% while the wall facing was externally braced. At the end of soil placement the external braces were removed and an initial static load condition established.

The soil reinforcement was a knitted polyester (PET) geogrid. Numerical modelling of reinforced soil walls (Rowe and Ho 1998, Bathurst and Hatami 1998, Hatami *et al*. 2001) and results of instrumented reinforced soil walls in the field under static loading conditions (Allen and Bathurst 2002) have clearly identified that reinforcement stiffness (rather than tensile strength at rupture) is a key parameter to accurately predict reinforcement loads under typical operational conditions. Therefore, the reinforcement material was selected to have a tensile stiffness that when scaled to prototype scale represents a typical geogrid material used in field walls.

An instrumented footing was used to decouple vertical and horizontal toe load components of the

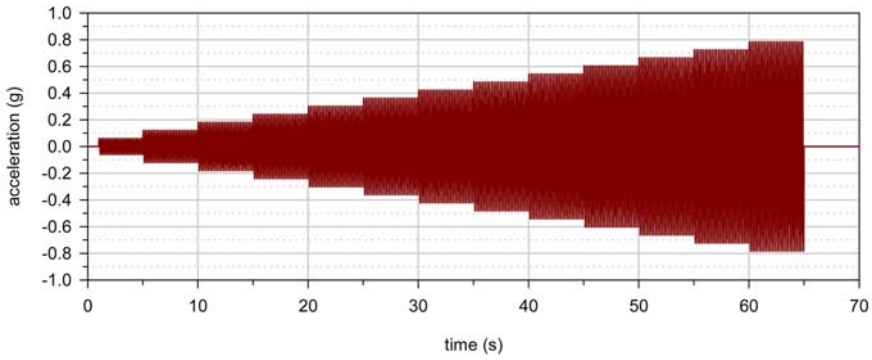

Fig. 2 Target base accelerogram (stepped constant amplitude sinusoidal function with frequency = 5 Hz)

facing panel. For the sliding toe model the horizontal load cells at the wall toe were removed after construction (Fig. 1). The horizontal movement of the wall facing was measured using displacement potentiometers mounted against the facing panel on the shaking table platform. Reinforcement strains were measured using strain gauges that were bonded directly to the polyester geogrid longitudinal members and extensometers that were attached to selected geogrid junctions. Acceleration response during shaking was measured using two accelerometers attached to the facing panel and four accelerometers buried at different locations in the backfill.

The target horizontal base acceleration was a stepped-amplitude sinusoidal function with a frequency of 5 Hz (Fig. 2). The excitation record was applied in 0.05 g increments of 5 seconds duration. The excitation stages were applied until excessive model deformation occurred. A stepped-acceleration amplitude base excitation record has been shown to be more aggressive than actual earthquake records scaled to the same peak acceleration in physical shaking table tests (Murata *et al*. 1994) and numerical modelling (Hatami and Bathurst 2001). However, a stepped record simplifies interpretation of dynamic wall response.

5. Numerical approach

The finite difference-based program FLAC (Fast Lagrangian Analysis of Continua) (Itasca 2005) was used to develop the plane strain numerical model and to simulate the static and dynamic response of the reinforced soil models. The backfill, facing panel and soil were modelled as continuum zones (Fig. 3). The reinforcement layers were modelled with two-noded one-dimensional structural cable elements with tensile strength and negligible compressive strength. The reinforcement layers were rigidly attached to the corresponding grid point on the back of the facing panel zone matching the attachment detail in the physical models.

The model wall foundation in the numerical model was assumed to be rigid. The back of the wall (i.e. far-end boundary) was modelled using a rigid zone. The model wall facing toe boundary condition was modelled with two-noded one-dimensional beam elements with three plastic hinges (Fig. 3(b)). The numerical mesh size in Fig. 3(a), was selected based on a series of preliminary numerical analyses to concurrently optimize numerical accuracy and computation time. Five to six rows of soil zones were used between reinforcement layers to prevent numerical effects due to coarse level of discretization. Large strain mode was used in the model to account for large

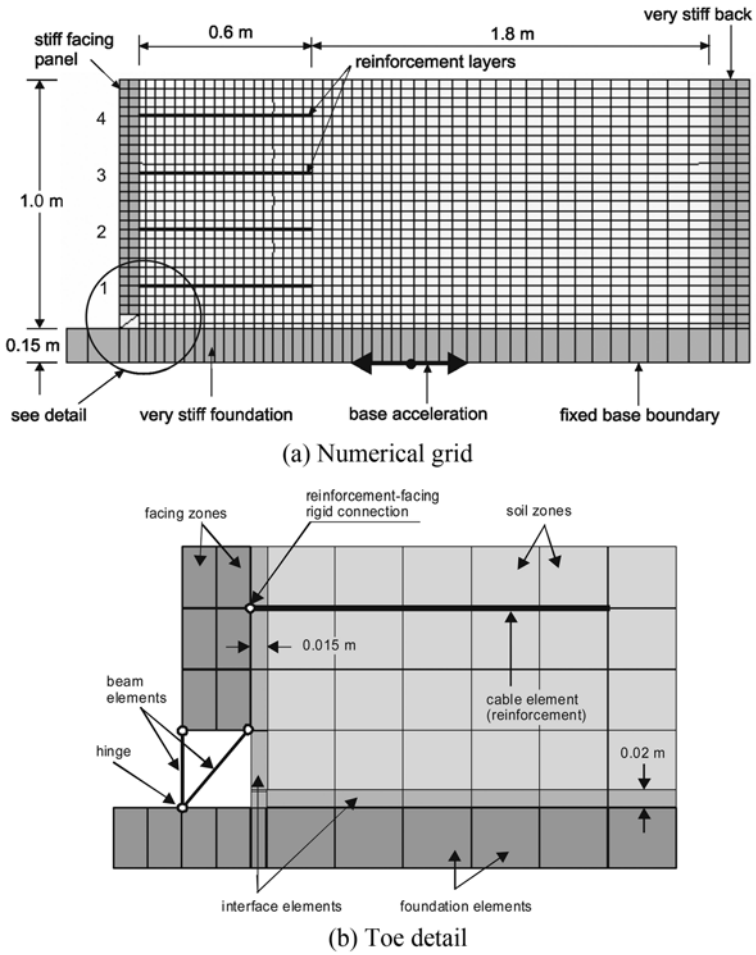

Fig. 3 FLAC model of reinforced soil wall with hinged toe boundary condition

deformations.

The numerical grid was constructed in layers to simulate soil placement. However, there was no significant difference in numerical results by constructing the entire numerical domain instantaneously. This outcome may be expected since the wall facing in the physical tests was braced during construction. Sequential numerical construction is important to accurately simulate wall response if the wall facing column is constructed sequentially with no external support as is the case for modular block walls as demonstrated by Huang *et al*. (2009). The models were brought to static equilibrium following removal of the external props. Next, the full width of the foundation and back wall of the numerical model were subjected to the velocity-time record computed from the measured base acceleration record applied to the physical shaking table model.

For the case of numerical simulation of reinforced soil walls under static load conditions, both Ling (2003) and Huang *et al*. (2009) have demonstrated that increasing the complexity of constitutive models for component material properties does not guarantee improved simulation accuracy. Zarnani and Bathurst (2008, 2009a) carried out a series of numerical simulations of physical seismic buffer tests using the same shaking table and model size as reported here. They showed that up to about

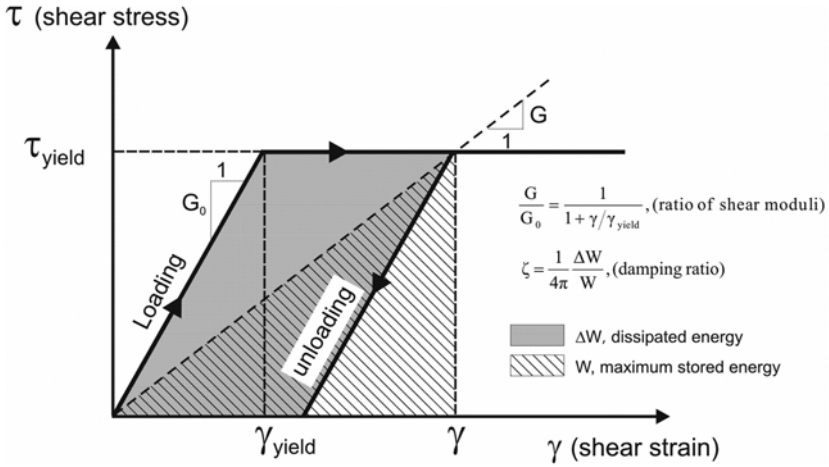

Fig. 4 Cyclic loading in elastic-plastic model with Mohr-Coulomb failure criterion (after Zarnani and Bathurst 2009a)

0.7g peak base excitation there was no practical advantage of using the well-known equivalent-linear method (ELM) (first introduced by Seed and Idriss 1969) for the soil, compared to the same linear-elastic plastic M-C model used in the current study. The explanation for this apparent contradiction is that hysteretic unload-reload behaviour, nonlinear shear modulus degradation of the soil and increasing damping with increasing shear strain that are explicit components of the ELM approach is a natural outcome at post-yield using the linear elastic-plastic M-C model (e.g. Itasca 2005, Ishihara 1996, Wood 2004) (Fig. 4). Based on prior experience with numerical modelling of the simulated seismic response of seismic buffer tests using the same shaking table and the same soil backfill, the numerical simulations in the current study were carried out using a simple linear elastic M-C model. The predictions using this simple soil constitutive model are shown later in the paper to do very well in most cases.

6. Material properties

6.1 Soil properties

The soil was modelled as a cohesionless material with linear elastic-plastic response, Mohr-Coulomb (M-C) failure criterion and dilation angle. The values of peak friction angle and dilation angle were first estimated from boundary loads and displacements measured in conventional laboratory direct shear box tests with soil prepared to a unit weight of 15.7 kN/m^3 (i.e. matching the wall model tests). However, the 2-D numerical model of reinforced soil walls in FLAC requires plane strain soil parameters as input values. For example, the peak shear strength of dense frictional sand is greater under plane strain conditions than values deduced from direct shear conditions (Bolton 1986). The peak soil friction angle measured from direct shear tests (51 degrees) was increased to 58 degrees using the Bolton equation. The soil initial shear modulus, G_o, and initial bulk modulus, K_o were adjusted until the equivalent stress-deformation response of the FLAC model (Fig. 5(a)) gave a good fit to physical test results (Fig. 5(b)). During this calibration, the dilation

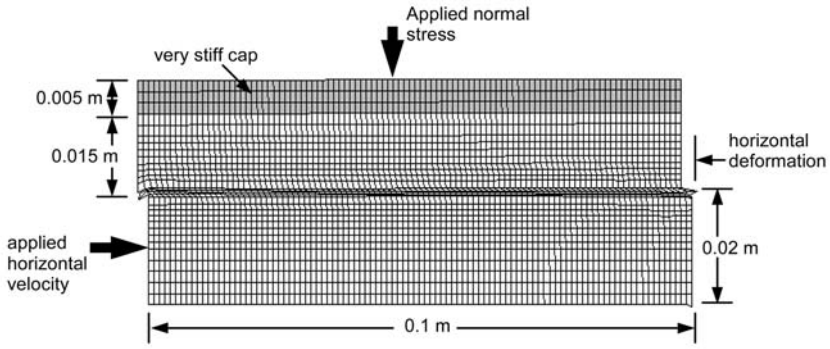

(a) Deformed two-dimensional FLAC numerical model of direct shear box test

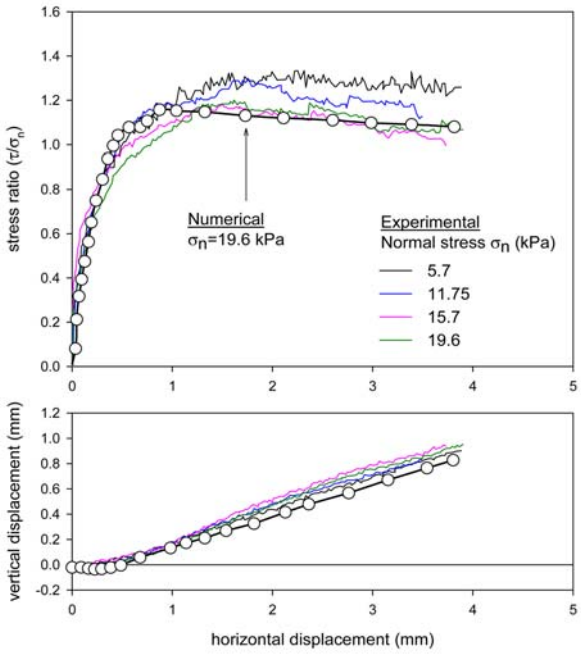

(b) Normalized stress-displacement response of physical and numerical tests

Fig. 5 Direct shear box tests on sand

angle, Ψ was kept constant. It is interesting to note that the numerical soil shear-stress displacement response deduced at the test boundaries (Fig. 5(b)) matches the strain softening in the physical test despite the use of the linear elastic-plastic M-C constitutive soil model. However, this can be explained by the observation that not all soil elements were at a plastic state at post-peak strength in the numerical model. Soil shear properties deduced from the combination of physical direct shear box tests and simulations are summarized in Table 1(a). These values were used in the reinforced soil wall simulations. The table also reports the measured sand residual friction angle from physical direct shear box tests as 46 degrees. However, a residual friction angle was not used in the numerical model nor was soil strain softening assumed in order to minimize the number of model parameters. Cyclic shear box testing at a model frequency of 5 Hz was not required since the peak

Table 1 Backfill soil and reinforcement material properties used in numerical modelling

(a) Backfill soil

Properties used in numerical model	Value
Unit weight, γ	15.7 kN/m^3
Cohesion	0
Plane strain peak friction angle, ϕ_{ps}	58°
Dilation angle, ψ	14.5°
Shear modulus, G_o	7 MPa
Bulk modulus, K_o	6 MPa

Note: residual friction angle of sand computed as 46 degrees but not used in constitutive soil model

(b) Reinforcement material

Properties	Values
Elastic modulus, $E = J/t$	45000 kPa
Yield strength, $f_{yield} = T_{rupture}/t$	6500 kPa
Compressive strength	0
Cross section area	0.002 m^2
Cross-section perimeter	2 m

Notes: Axial stiffness J at 2% strain = 90 kN/m and tensile rupture strength $T_{rupture}$ = 13 kN/m from wide-width strip tensile tests; thickness of geogrid taken as t = 2 mm.

friction angle of sand material under cyclic loading has been demonstrated to be unchanged from the value deduced from static loading conditions (Bathurst *et al*. 2002, Ishihara 1996, Prakash 1981).

6.2 Reinforcement

The reinforcement material was modelled using linear elastic-plastic cable elements with no compressive strength (Table 1(b)). Based on a review of experimental data for geogrid reinforcement materials at small strain, the influence of soil confinement on tensile properties of these materials is negligible (Shinoda and Bathurst 2004, Walters *et al*. 2002) and the axial stiffness (modulus) for polyester geogrids is sensibly rate-of-strain independent (Bathurst and Cai 1994). Therefore, the stiffness properties of the geogrid reinforcement in this investigation were determined from in-isolation, rapid strain-rate (i.e. 6, 12 and 22% strain/min) tensile tests. In a separate series of tensile tests, strain gauges were bonded directly to longitudinal members. A linear curve was fitted to the tensile load-strain data up to about 2% strain (Fig. 6). Tensile strains varied between parallel longitudinal members which explains the spread in data points. A first-order linear equation and prediction limits at ± 2 standard deviations were fitted to the data and used later to compute reinforcement loads and to provide an estimate of load prediction accuracy.

6.3 Mass and stiffness damping

To avoid low-level oscillation, stiffness and mass proportional Rayleigh damping in conjunction with hysteresis damping was used (Itasca 2005). In this study, a constant damping ratio of ξ = 5%

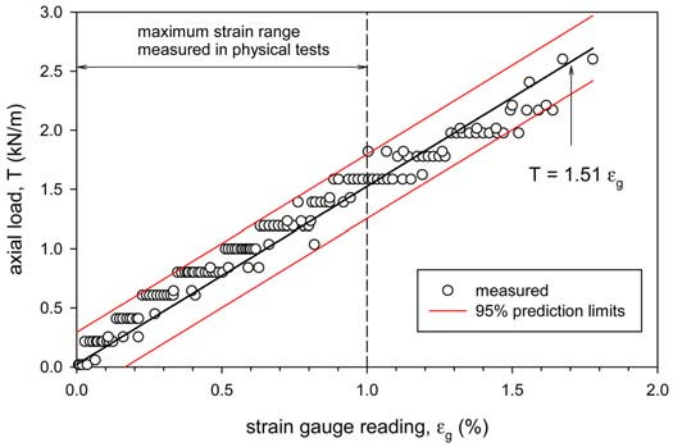

Fig. 6 Calibration of axial load-strain gauge response for polyester geogrid reinforcement at low strain

was selected and assigned to backfill soil and facing elements only. A parametric numerical study of a 6-m high GRS wall model by Bathurst and Hatami (1998) showed that there was only a small effect on dynamic model response (facing displacement and reinforcement load) for damping ratios in the range of 5% to 10%. Nevertheless, the choice of damping type and magnitude can be expected to influence numerical outcomes as demonstrated in other related work (Bathurst and Hatami 1998, Lee *et al*. 2010, Ling *et al*. 2010).

6.4 Boundaries

Four-noded, linear elastic continuum zones were used to model the full height-rigid-facing panel, shaking table and far-end boundary. These zones were assigned unit weight, shear modulus and bulk modulus values of 17.2 kN/m^3, 1000 MPa, and 1100 MPa, respectively. It was found that larger values of bulk and shear modulus for the facing panel resulted in numerical instability due to the large difference in these values and values for the adjoining soil zones.

6.5 Interfaces

The reinforcement (cable) elements in the numerical model were attached to soil grid points to simulate a perfect bond. This attachment ensured compatibility of displacement between reinforcement structural nodes and backfill soil grid points. As noted later in the paper, possible slip between the soil and top reinforcement layer in the physical tests may have contributed to relatively less accurate reinforcement load prediction. However, in the absence of physical test data to guide the selection of interface stiffness values a perfect bond simplifies the modelling and interpretation of results.

The interface between the backfill soil and the foundation was modelled using a thin (0.02 m thickness) soil layer placed directly on the foundation (Fig. 3). The material properties of this layer were the same as those of the backfill material consistent with the rough sand bottom (glued layer of sand) in the physical tests.

The interface between the reinforced soil and the facing panel was modelled using a thin (0.015 m thick) soil column directly behind the facing panel (Fig. 3). The soil-facing panel interface material

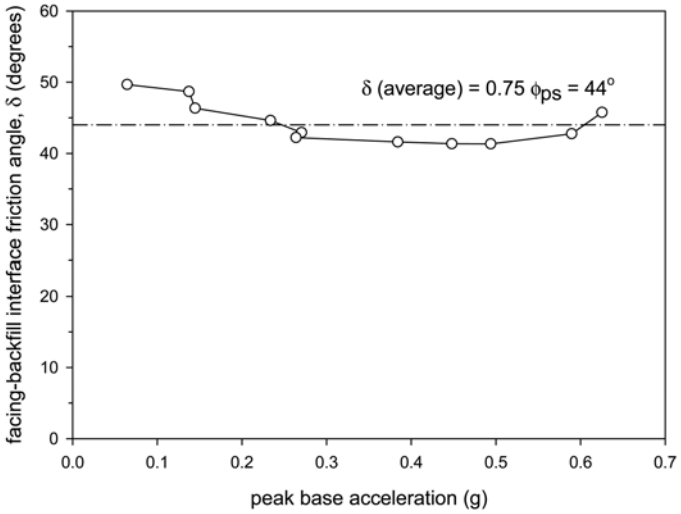

Fig. 7 Variation of back-calculated facing panel-backfill interface friction angle with peak input base acceleration amplitude (from physical test with hinged toe)

properties were the same as the backfill properties except for the friction angle (δ). This value was computed at peak base acceleration intervals from measured loads in the physical test wall with a hinged toe according to the following equation

$$\delta = \tan^{-1}\left(\frac{R_V - W_f}{R_H + \Sigma T_i} \right) \tag{1}$$

Here, R_V and R_H are the measured vertical and horizontal components of the toe reaction, respectively, W_f is the weight of the facing panel, and ΣT_i is the sum of the total horizontal component of connection loads. Back-calculated values are shown in Fig. 7. A value of δ = 0.75 ϕ_{ps} = 44° was judged to be reasonable and was implemented in all numerical simulations.

7. Comparison of numerical and physical test results

As noted earlier in the paper, the physical tests were continued to a peak base excitation of about 0.8 g corresponding to test durations of about 65 seconds (Fig. 2). The numerical simulations were terminated after about 50 to 55 seconds due to numerical instability. However, at the end of numerical simulations, the peak base excitations were in excess of 0.3 g which is judged to be a significant dynamic load particularly when the excitation record has stepped sinusoidal amplitude. The data points in some of the plots to follow correspond to values at peak positive acceleration in the direction from the soil towards the wall facing.

7.1 Model wall fundamental frequency

An often over-looked response feature of soil-structures is the fundamental frequency of the system. In design practice it is desirable that the predominant frequency of the input motion (design

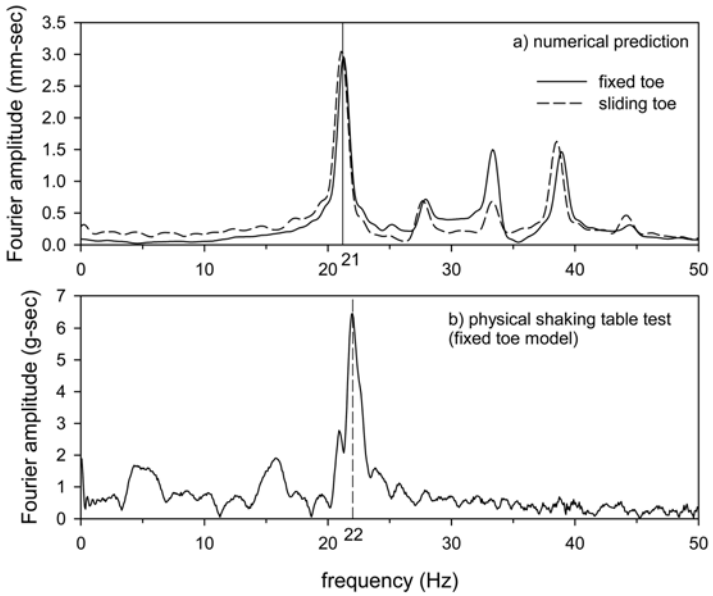

Fig. 8 Free vibration frequency response of numerical and physical reinforced soil model walls with full-height rigid panel facing (after El-Emam and Bathurst 2004)

earthquake) be different from the model wall fundamental frequency to prevent premature failure due to a resonance condition (e.g. Zarnani and Bathurst 2009b). Retaining walls of typical height (say $H < 10$ m) are short-period structures and thus their seismic response is dominated by their fundamental frequency (Hatami and Bathurst 2000). In the current study, fundamental frequency was determined experimentally for the hinged toe model (El-Emam and Bathurst 2004) and numerically using the free vibration method. In the numerical simulations the model walls were subjected to a sinusoidal input excitation with predominant frequency of 5 Hz for about 6 seconds. Then the models were allowed to vibrate freely with zero input acceleration. The frequency response of the models with respect to acceleration and wall displacement was monitored during the free vibration stage and the fundamental frequencies identified as shown in Fig. 8. The values of fundamental frequency calculated from experimental and numerical free vibration tests were similar (i.e. $f_{11} = 22$ and 21 Hz, respectively). Fig. 8(a) shows that the model wall toe boundary condition has negligible effect on the magnitude of the fundamental frequency in numerical simulations which is consistent with previous parametric numerical analyses reported by Hatami and Bathurst (2000). The fundamental frequency values are very close to the values of 21 to 22 Hz predicted using closed-form solutions based on elastic theory (e.g. Wu and Finn 1996). Furthermore, these values are well above the input excitation frequency of 5 Hz which means that the response of the physical and numerical models in this study is not complicated by close proximity to the fundamental frequency of the systems.

7.2 Wall facing displacements

Post-construction predicted and measured time histories of the peak lateral displacement at the top of the wall facing panel for hinged and sliding toe model walls are shown in Figs. 9(a) and 9(b),

respectively, and at the base of the sliding toe model in Fig. 9(c). The predicted lateral displacements at the top and bottom of the sliding toe wall are judged to be in good agreement with the experimental data. The predicted top lateral displacements of the hinged toe model wall (Fig. 9(a)) show very good agreement with the measured data up to about 35 seconds; thereafter numerical simulation results become progressively greater.

The results in Fig. 9 show that both hinged and sliding toe model walls experienced a large increase in rate of lateral deformation at about 35 to 40 seconds from the start of the tests when the measured input base acceleration amplitude became greater than 0.25 g to 0.3 g. This *critical*

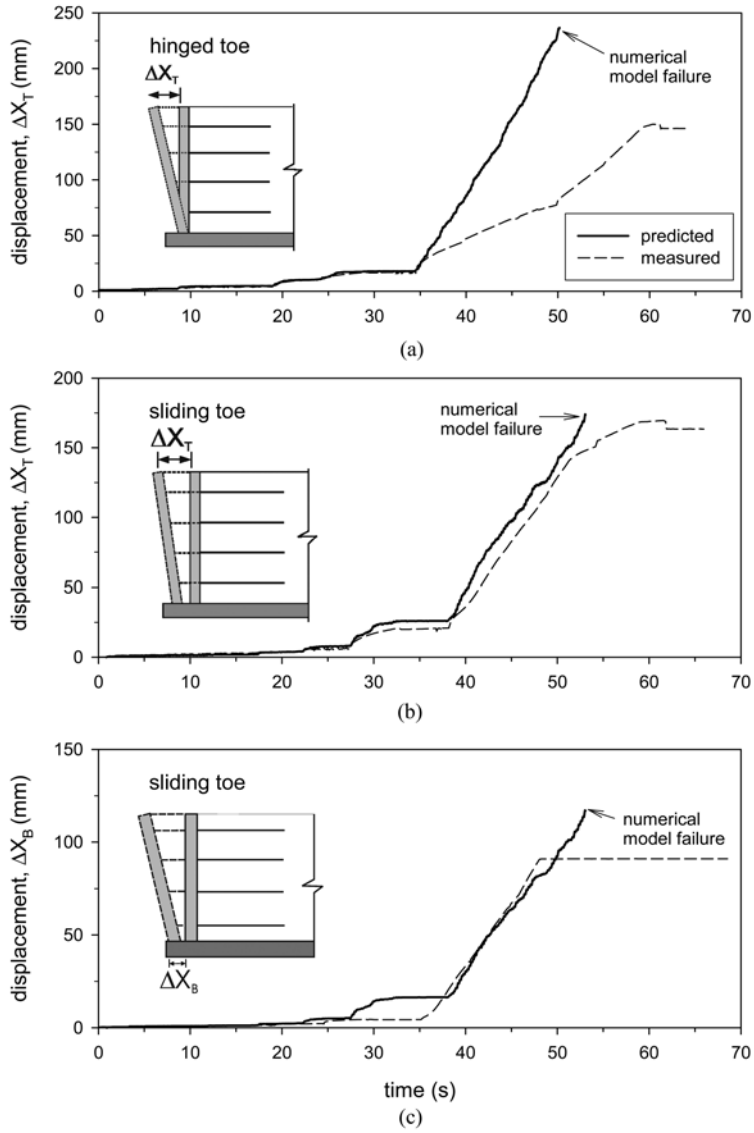

Fig. 9 Predicted (numerical) and measured time histories for lateral displacement at: (a) top of facing panel for hinged toe model and (b) top of facing panel for sliding toe model and (c) bottom of facing panel for sliding toe model

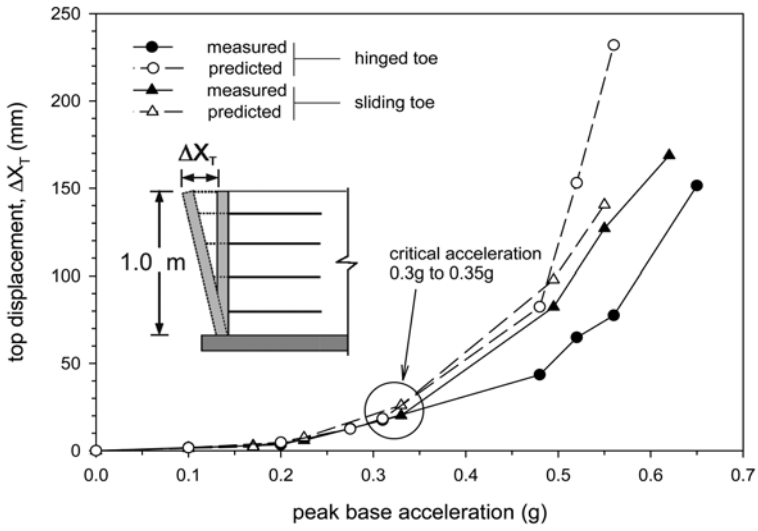

Fig. 10 Predicted and measured maximum lateral displacement at the top of facing panel versus peak input base acceleration

acceleration is highlighted in Fig. 10 using peak base acceleration as the independent parameter. Sharp increases in displacement versus peak base acceleration can be found in the literature for similar reduced-scale model shaking table tests of conventional walls, and soil reinforced retaining walls and abutments (Tatsuoka *et al*. 2009, Murata *et al*. 1994). Sakaguchi *et al*. (1992) carried out shaking table tests on 1.5-m high geosynthetic reinforced soil wall models with block facing treatments and reported critical acceleration amplitudes in the range of about 0.3 g to 0.4 g when soil response was judged to have changed from elastic to plastic behaviour. The numerical models for both walls in the current study are judged to have predicted the critical acceleration reasonably well. However, the post-critical acceleration responses are close for the numerical simulations but dissimilar for the two physical tests. For example, the hinged toe model generated less deformation at the wall top. Furthermore, for base acceleration greater than 0.5 g, the predicted top wall displacements for the hinged toe model were greater than the sliding toe model which is the reverse trend for the physical tests.

7.3 Mass movements and ground motion amplification

Plots of shear zones within the reinforced soil and retained soil zones from the control wall (wall model 1) in the larger research program (El-Emam and Bathurst 2004) and the matching numerical hinged toe model are shown in Fig. 11. This was the only wall which included instrumentation to detect internal soil failure mechanisms at the end of base excitation. The numerical simulation was carried out using the same approach and constitutive models described earlier. The numerical results show the development of a wedge of soil that grows from a single wedge to a larger bi-linear wedge with increasing base acceleration. This mechanism is clear from numerical modelling but was not easily detectable during physical testing. The exception is Fig. 11(d) close to the end of the base shaking. In this physical test an array of thin flexible plastic tubes was inserted through the height of the soil and then filled with a resin after the test was completed. The hardened resin

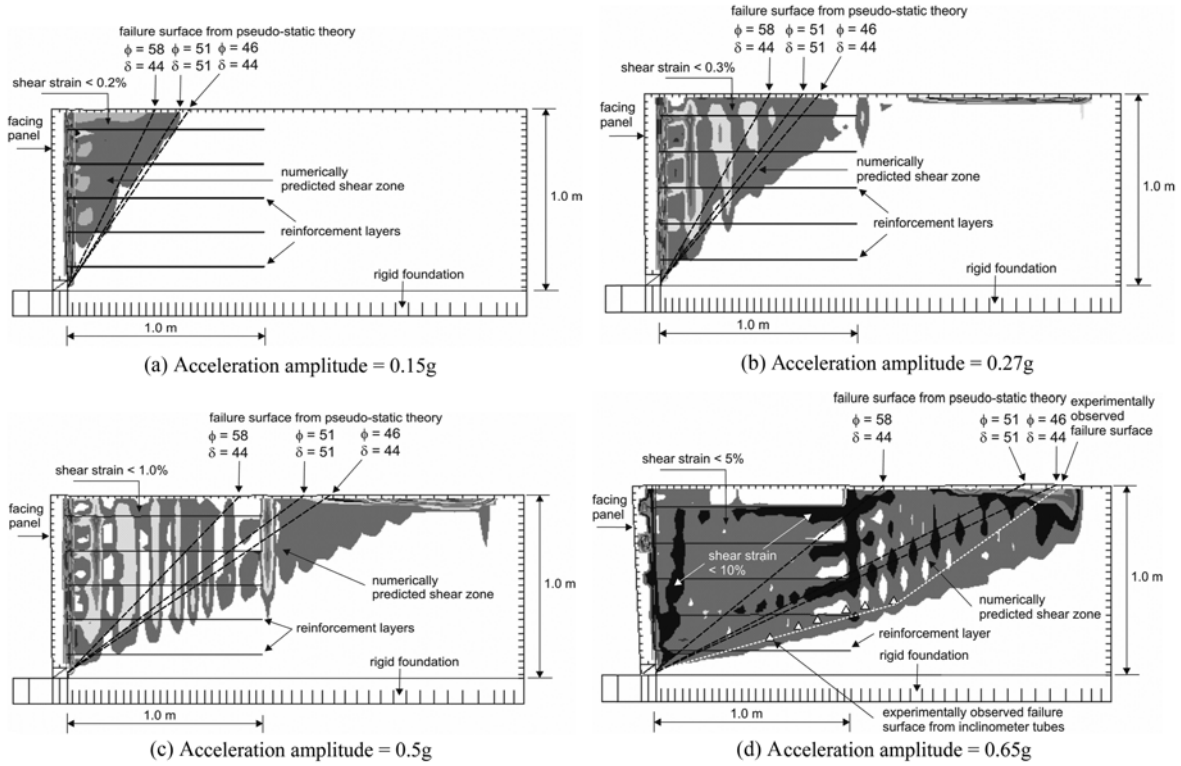

Fig. 11 Predicted (numerical) and observed soil failure zone surfaces for hinged toe condition (model wall 1). Note: Dark shading indicates zones of relatively large shear strain

captured (froze) the location of major soil disturbance. When the failure surface points from these (inclinometer) tubes are connected to the observed failure scarp at the far end of the soil surface there is judged to be a reasonably good agreement with the bottom of the soil shear zone predicted by the numerical model.

The reinforced soil zone can be observed to have deformed as a parallelogram indicating that the combination of rigid facing panel, soil and reinforcement layers creates a monolithic block. A swale at the soil surface at the end of the reinforcement zone was also observed in the physical test consistent with the block deformation pattern observed in the numerical simulation. A similar parallelogram block movement has been reported by Tatsuoka *et al*. (1998) from similar but smaller-scale reinforced soil wall tests with a rigid facing.

Superimposed on the figures are linear failure surfaces inclined at angle a_{AE} from the horizontal computed using a solution to Mononobe-Okabe earth pressure theory (Zarrabi 1979, Bathurst *et al*. 2002)

$$\alpha_{AE} = \phi - \theta + \tan^{-1}\left[\frac{-\tan(\phi-\beta-\theta)+a_2}{1+\tan(\delta-\omega+\theta)[\tan(\phi-\beta-\theta)+\cot(\phi+\omega-\theta)]}\right] \quad (2)$$

The parameter a_2 in Eq. (2) is given by

$$a_2 = \sqrt{\tan(\phi-\beta-\theta)[\tan(\phi-\beta-\theta)+\cot(\phi+\omega-\theta)][1+\tan(\delta-\omega+\theta)\cot(\phi+\omega-\theta)]} \quad (3)$$

Here, ϕ = soil friction angle, δ = wall-soil interface friction angle; ω = wall/slope face inclination (positive in a clockwise direction from the vertical); β = backfill surface inclination angle (from horizontal); and the seismic inertia angle $\theta = \tan^{-1}[k_h/(1 \pm k_v)]$. Quantities k_h and k_v are horizontal and vertical seismic coefficients, respectively, expressed as fractions of the gravitational constant, g. Calculations are simplified in this investigation because $\beta = k_v = \omega = 0$.

Three different combinations of soil friction angle and interface friction angle were investigated to see if the boundaries of the disturbed soil zone could be matched to failure surfaces predicted using Eq. (2). In all cases the single wedge computed using values of $\phi = 58^o$ and $\delta = 44^o$ (i.e. values used in the soil constitutive model) under-predicted the volume of the disturbed soil zone. Only at the end of the test was there a reasonable correspondence between the orientation of the physical observed failure surface in the retained soil zone and the failure surface orientation from the closed-form solution. Similar under-estimation of the volume of the shear zone has been reported by Koseki *et al*. (1998) in reinforced soil model wall shaking table tests and with numerical results (Bathurst and Hatami 1998).

Figs. 11(c) and 11(d) illustrate that the bottom reinforcement layers are important in resisting seismic forces at higher input base acceleration amplitudes. In this test the failure surface(s) propagated further from the wall facing with increasing base excitation and eventually fully contained the top reinforcement layers. Therefore, the seismic load was transferred to the bottom reinforcement layers which still had sufficient anchorage length within the resisting soil zone. An important conclusion from the numerical results is that the internal failure surface (based on a single wedge propagating from the wall toe) used for internal stability design in current design codes may under-predict the reinforcement length required to satisfy the pullout limit state.

Finally, the numerical model indicated that large strains occurred at the back of the facing panel (i.e. facing panel-soil interface) which is consistent with the numerical results obtained by Bathurst and Hatami (1998) and evidence of high connection loads presented later.

Ground motion amplification can vary up the height of an earth retaining wall structure depending on the height of wall, soil type and base excitation characteristics (Hatami *et al*. 2005, Nouri *et al*. 2008, Carotti and Rimoldi 1998, Matsuo *et al*. 1998, Ling *et al*. 2004, 2005b, Murata *et al*. 1994, Krishna and Latha 2007). Accelerometers were mounted on the shaking table and at different locations on the wall face and in the soil in the physical experiments (Fig. 1). The fast Fourier transform (FFT) was computed for each accelerometer record up to the end of the numerical simulation and from the matching numerical experiment for the same time interval and location in the physical test. Acceleration amplification is defined here as the ratio of the accelerometer FFT at locations above the shaking table to the accelerometer FFT record for the shaking table. Fig. 12 shows these ratios. The physical tests show that acceleration amplification increases with height above the table and is greater at the face than in the soil. Acceleration amplification is also greater for the sliding toe than for the hinged toe model at the same locations. The largest amplification ratios from the physical tests are in the range of 2.5 to 3. However, in the numerical tests the predicted values for both model walls are sensibly constant at about 1.1. Clearly, the numerical experiments behave more as a monolithic block than the physical experiments.

7.4 Reinforcement load-time histories

Examples of the predicted and measured time histories of the axial reinforcement load at the back

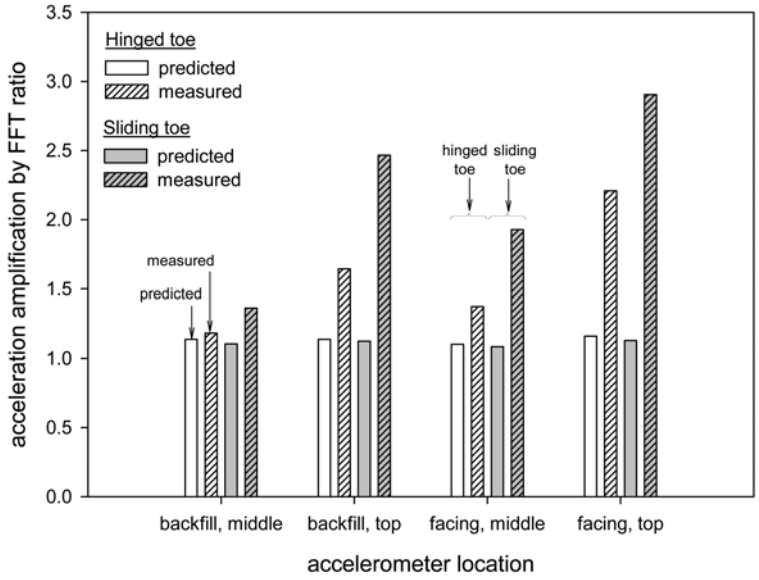

Fig. 12 Acceleration amplification

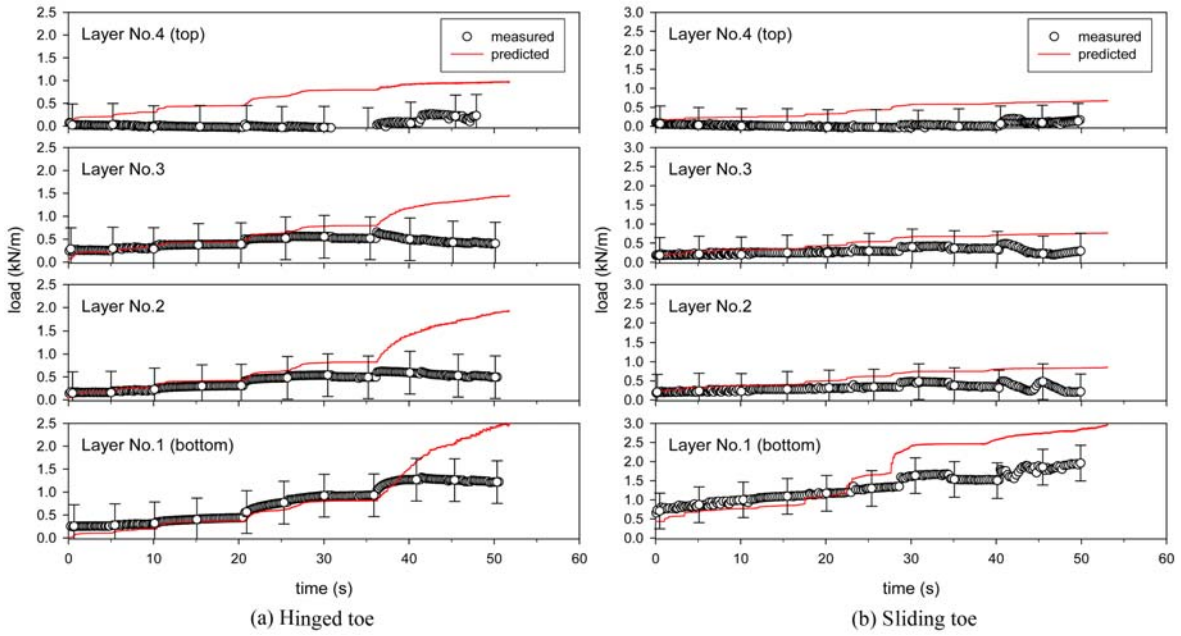

Fig. 13 Predicted (numerical) and measured reinforcement load-time history at facing-reinforcement connections. Note: Range bars are ± 1 standard deviation of measured loads

of the facing panel (i.e. connection loads) for both hinged and sliding toe model walls are shown in Fig. 13. The range bars in the figure represent ± 1 standard deviation of the estimate of reinforcement loads deduced from strain gauge readings close to the back of the facing (Fig. 6). The figures show that predicted connection loads accumulate with time during base shaking. With the exception of the

top reinforcement layers in both model walls, the numerical predictions are judged to be in satisfactory agreement with reinforcement connection loads for the first 25 seconds of the test, when base accelerations are ≤ 0.35 g. For base acceleration amplitudes greater than 0.35 g, the numerical model over-predicted the reinforcement connection loads for both hinged and sliding toe models. This may be due to slip between the reinforcement and sand soil due to low confining pressure in the physical tests which is not captured in numerical simulations using a perfect bond.

7.5 Reinforcement load distribution

Fig. 14 shows the measured and predicted reinforcement loads with distance from the back of the facing panel, at the end of construction and at different peak input base acceleration. Peak values at all locations were essentially time-coincident in both physical and numerical experiments. In most plots, the numerically predicted magnitude and distribution of reinforcement loads are judged to be in good agreement with the measurement data falling within ±1 standard deviation. The largest discrepancies between measured and predicted values are for the sliding toe model at relatively large base excitation (Fig. 14(d)) which is possibly due to low confining pressure in the physical 1-g models as noted earlier.

In most cases, the increase in tensile load in the vicinity of the facing panel is captured. This is believed to be due to down-drag of reinforcement layers when the soil behind the wall moves down as the facing moves outward. This phenomenon has been noted in hard-faced full-scale field walls (Allen and Bathurst 2006) and full-scale laboratory model walls (Bathurst *et al*. 2000) at the end of construction. It is also possible that additional load was developed at the connections due to out-of-phase lateral displacement of the facing panel and the soil backfill.

7.6 Distribution of connection and toe loads

The distribution and magnitude of the measured and predicted reinforcement connection loads are plotted in Figs. 15 and 16 for hinged and sliding walls, respectively, at the end of construction (i.e. static loading) and at different input base accelerations (i.e. dynamic loading). The peak connection loads in both numerical and physical tests are time-coincident. The range bars represent ± 1 standard deviation of measured loads as discussed in previous sections. Superimposed on the figures are the connection loads calculated using three different seismic design methods for geosynthetic reinforced soil walls (i.e. Bathurst and Cai 1995, NCMA 2009 and FHWA 2009, AASHTO 2010).

The analysis method for reinforced soil walls proposed by (Bathurst and Cai 1995) assumes a distribution of internal earth pressure and assigns reinforcement load to each reinforcement layer in proportion to the tributary area, S_v corresponding to that layer. In addition, the inertial force due to the contributory portion of the facing column, $k_h \Delta W_f$ is added to the reinforcement loads under seismic loading. Hence the total tensile load, T, in the reinforcement layer is calculated as

$$T = T_{sta} + k_h \Delta W_f + T_{dyn} \tag{4}$$

In Eq. (4), the quantity $\Delta W_f = S_v L_f \gamma_f$ is the weight of the facing panel increment falling within the contributory area, S_v of the reinforcement layer. Parameters L_f and γ_f are the facing panel width (toe to heel) and unit weight, respectively. Quantity k_h is the horizontal seismic coefficient expressed as a fraction of the gravitational constant, g. The static component, T_{sta} of the reinforcement load is

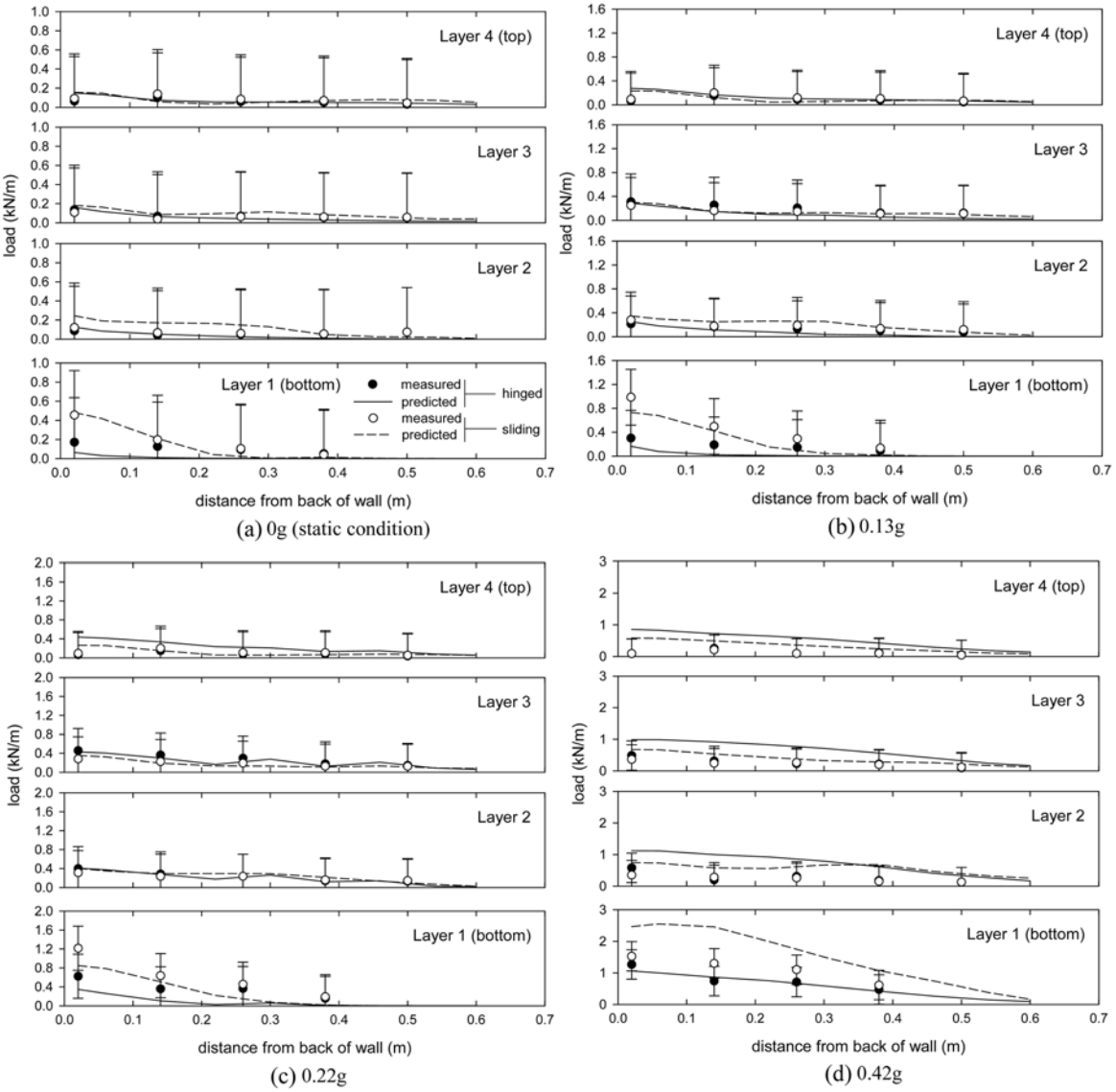

Fig. 14 Predicted (numerical) and measured reinforcement loads at static condition (end of construction) and at selected peak input base acceleration. Note: Range bars are ± 1 standard deviation of measured loads

calculated as follows

$$T_{sta} = K_{AH}\gamma z S_v \tag{5}$$

where γ is soil unit weight and z is distance from the crest of the wall to the reinforcement layer. The additional earth pressure beyond the static pressure (dynamic earth pressure) is assumed to be trapezoidal shaped with larger dynamic pressure at the top of the wall than at the bottom. The corresponding dynamic component, T_{dyn} of the reinforcement load is calculated as follows

$$T_{dyn} = \left(0.8 - 0.6\frac{z}{H}\right)\Delta K_{dyn(H)}\gamma H S_v \tag{6}$$

where $\Delta K_{dyn(H)}$ is the equivalent pseudo-static coefficient of dynamic load. Details are given in the paper by Bathurst and Cai (1995).

In Eq. (5), the quantity, K_{AH} is the horizontal component of the static earth pressure coefficient, calculated from Coulomb earth pressure theory. The calculation of dynamic components, T_{dyn} of reinforcement load in Eq. (6) is based on the assumption that the resultant of the dynamic component is located at 0.6H above the base of reinforced soil mass (Bathurst and Cai 1995) which is consistent with the pseudo-static design of anchored sheet pile walls (Ebling and Morrison 1993). As a consequence of this assumption, the relative proportion of load carried by uniformly spaced reinforcement layers closest to the crest of a wall increases with increasing horizontal acceleration. The NCMA (2009) design guidance document simplifies Eq. (6) by removing the term in brackets. This is equivalent to a uniform dynamic pressure increment at the back of the wall facing.

FHWA (2009) and AASHTO (2010) guidelines use different procedures to calculate and assign reinforcement loads to each reinforcement layer. In the FHWA (2009) method the dynamic earth load is calculated as $\Delta P_{dyn} = k_h W_A$, where W_A is the weight of the static internal failure wedge. The dynamic load increment is distributed to each reinforcement layer evenly. Both the FHWA (2009) and NCMA (2009) methods give the same solution for the case of uniform reinforcement spacing (S_v). For the AASHTO (2010) method, the distribution of the dynamic load increment, ΔP_{dyn} between the reinforcement layers is weighted based on the total anchorage length embedded in the resistance zone. Therefore, the reinforcement dynamic load increment, T_{dyn} is calculated according to

$$T_{dyn} = \Delta P_{dyn} \frac{L_a}{\sum_{n} L_a} \tag{7}$$

where: n = number of reinforcement layers; and L_a = anchorage length of the reinforcement layer (i.e. the portion of the layer extended beyond the failure surface). This approach leads to redistribution of dynamic load to the lower reinforcement layers for internal stability calculations in structures with uniform reinforcement length. Hence, the AASHTO method is less likely to result in an increased number and length of reinforcement layers at the top of the reinforced soil wall with increasing horizontal acceleration, which may be the case using the Bathurst and Cai (1995), FHWA (2009) and NCMA (2009) approaches.

Fig. 15 shows that the accuracy of predicted (numerical) connection loads for the hinged toe model wall is reasonably good for base acceleration amplitudes up to 0.3 g. The distribution of connection loads using closed-form solutions also fall within ± 1 standard deviation of measured values for acceleration amplitudes up to 0.3 g. However, at 0.43 g input base acceleration (Fig. 15(e)) only the AASHTO (2010) method predicts loads that fall consistently within measurement range bars. Nevertheless, none of the analytical methods consider the contribution of toe restraint to wall load capacity which is significant in this case. For example, the measured toe load was larger than the best-estimate of reinforcement load at all base excitation stages demonstrating that a horizontally restrained toe can attract significant wall force and possibly reduce the load demand on the reinforcement layers. Hence, the good agreement between measured and analytical predictions may be fortuitous. The potential load capacity of a restrained or partially restrained toe at end of

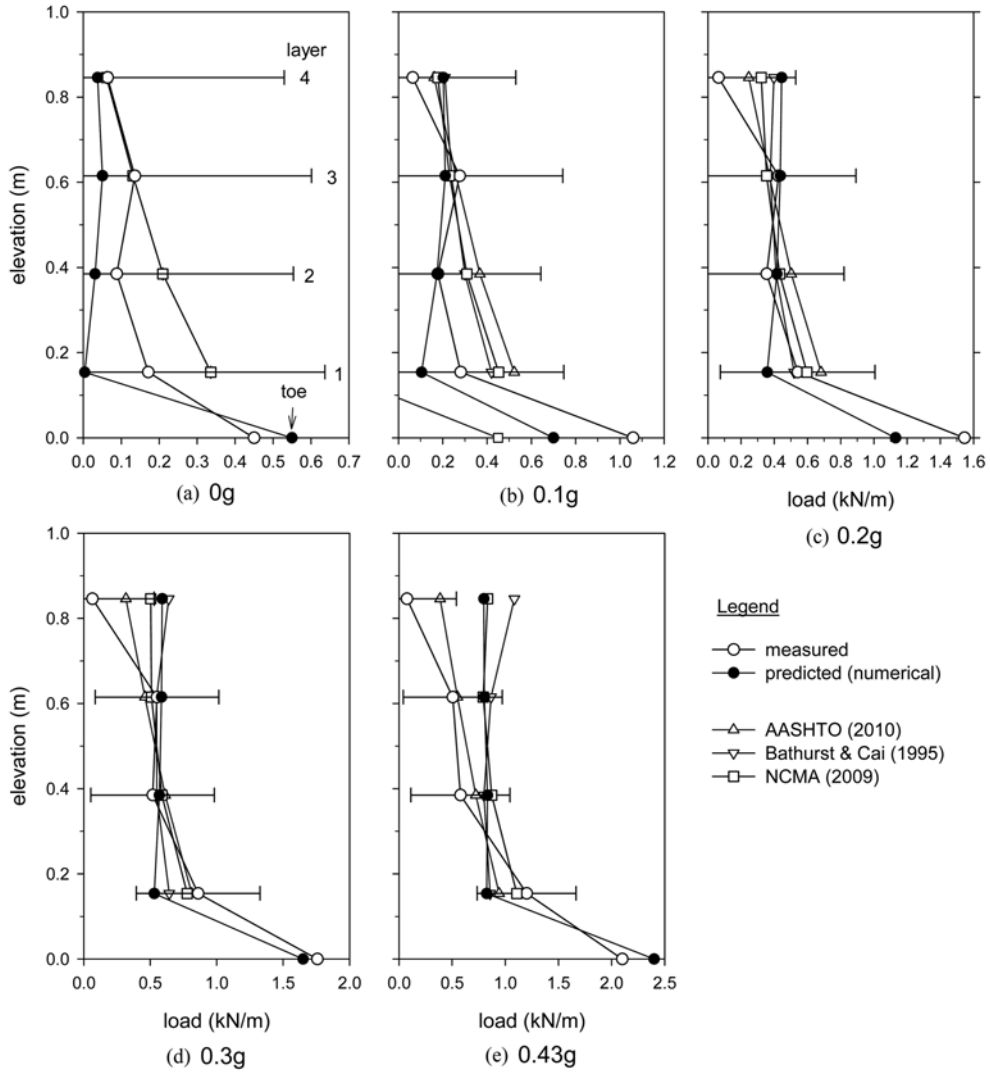

Fig. 15 Connection loads and horizontal toe loads at different peak input base acceleration for hinged toe model wall. Note: Range bars are ± 1 standard deviation of measured loads

construction (static load conditions) for walls with a hard facing has been demonstrated in full-scale physical wall tests (Bathurst *et al*. 2006) and in numerical parametric analyses (Huang *et al*. 2010).

The numerical and measured connection loads for the sliding toe model wall (Fig. 16) are in good agreement except for the bottom-most layer at the highest acceleration shown. Numerical and physical test results show that without the restraint offered by the wall toe much larger loads are carried by the lowermost reinforcement layer. However, the analytical solutions tend to increasingly over-estimate the top reinforcement layer load as base acceleration increases. Of the three analytical methods used, it can be argued that the AASHTO (2010) approach is most accurate when compared to the physical test results, but nevertheless under-estimates load in the bottom-most layer.

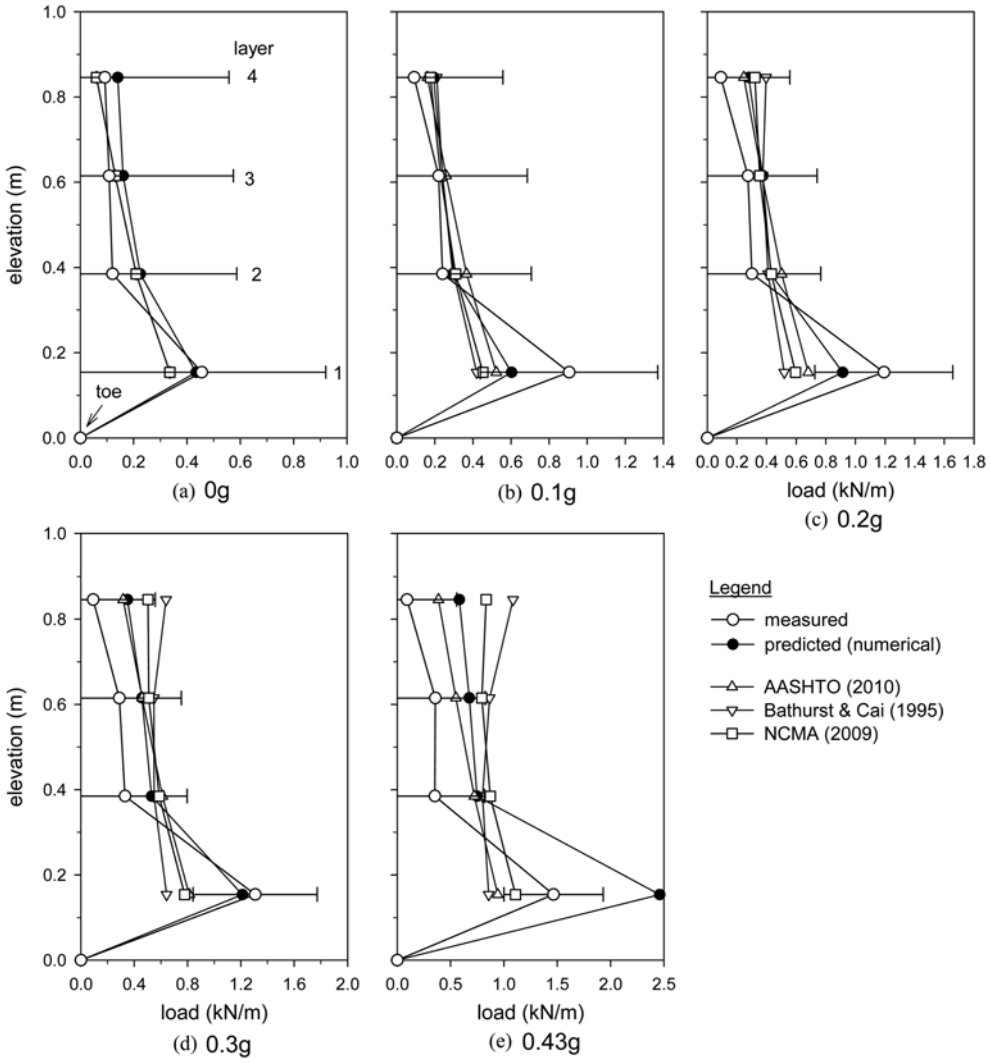

Fig. 16 Connection loads and horizontal toe loads at different input base acceleration amplitudes for sliding toe model wall. Note: range bars are ± 1 standard deviation of measured loads

7.7 Toe loads

Time histories of the measured and predicted vertical toe load for the sliding toe model wall are shown in Fig. 17(a). Vertical and horizontal toe load responses for the hinged toe model wall during base excitation are shown in Fig. 17(b). The predicted qualitative trends in vertical and horizontal toe loads are judged to be in satisfactory agreement with the measured values for both model walls during base excitation. However, there is under-prediction of toe loads early in the tests and over-prediction at longer times. For both walls, the self-weight of the facing panel is much less than measured and predicted vertical loads at the wall toe due to soil down-drag at the back of the wall facing. It can be seen that the numerical simulations captured the trend of slightly higher magnitude

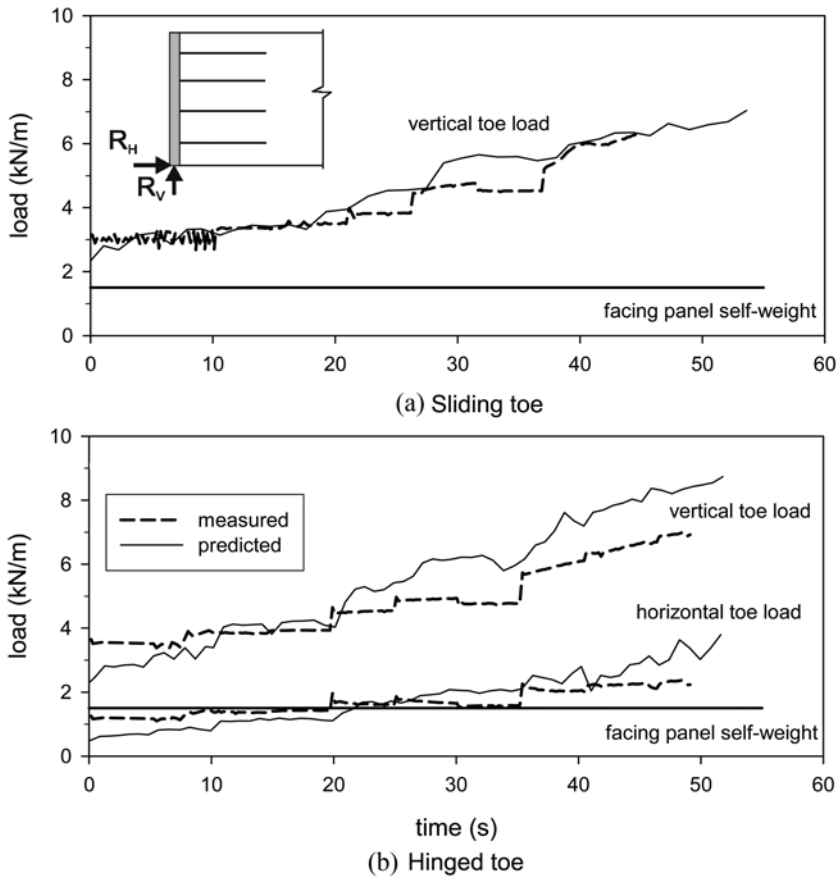

Fig. 17 Predicted (numerical) and measured time histories of the vertical and horizontal toe loads for hinged and sliding toe model walls

of the vertical toe load measured for the hinged toe model wall compared to the sliding toe model wall during shaking. The greater magnitude of the vertical toe load in the hinged toe model is consistent with a larger soil mass that rotated outward above the heel of the wall facing (i.e. compared to sliding toe case).

7.8 Earth load magnitude

The variation of measured total earth load acting against the facing panel with base acceleration is compared to numerical modelling results in Fig. 18 for both hinged and sliding toe model walls. The total earth load was calculated as the summation of all reinforcement connection loads (i.e. ΣT_i) in the sliding toe model wall, and as the summation of reinforcement connection loads plus the facing toe horizontal reaction (i.e. $\Sigma T_i + R_H$) in the hinged toe model wall.

Within the accuracy of the experimental measurements, the predicted horizontal earth forces at the back of the facing panel obtained from numerical models are in agreement with the measured data for the hinged toe model wall for base accelerations up to (say) 0.35 g. However, the predicted earth

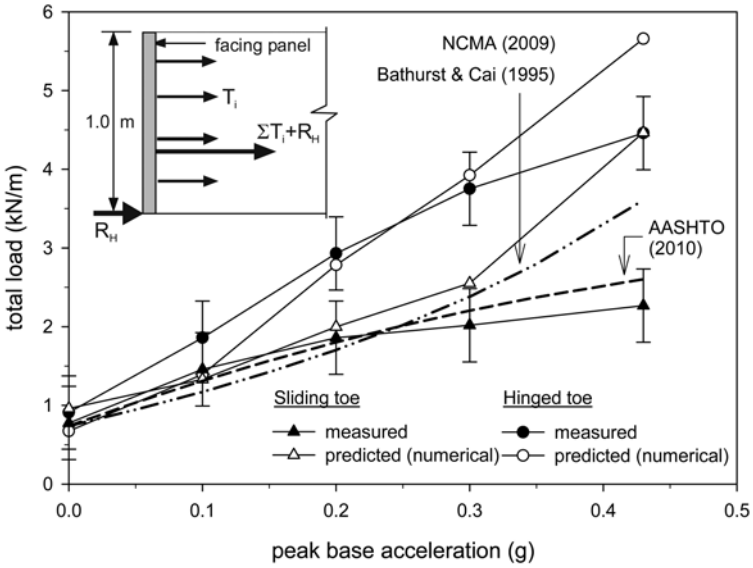

Fig. 18 Total load (reinforcement layers plus horizontal toe load) versus peak input base acceleration. Note: Range bars are ± 1 standard deviation of measured load

load values for the sliding toe model subjected to strong base shaking (e.g. > 0.3 g) are greater than measured values. The difference between the predicted and measured total earth forces behind the facing may be attributed to the slippage of reinforcement within the backfill soil which results in lower reinforcement connection loads compared to the (numerical) case when the slippage of reinforcement is prevented. The results shown in Fig. 18 indicate that closed-form seismic design solutions under-estimate measured and predicted values of the total earth load behind the hinged toe model wall. However, for the sliding toe model wall, the calculated values based on analytical methods fall between measured and numerically predicted total earth load values with the AASHTO (2010) values doing very well when compared to physical test results only.

8. Conclusions

This paper describes the results of numerical modelling of two nominally similar reduced-scale reinforced soil wall models tested on a shaking table and varying only with respect to boundary toe condition. The physical test walls were heavily instrumented. The numerical simulations were carried out using the commercially available dynamic finite difference program FLAC (Itasca 2005). Direct shear laboratory tests were modelled using FLAC to back-calculate input material properties for the soil and in-isolation tensile tests were carried out to characterize the load-strain properties of the reinforcement material. The model walls were subjected to the same input base acceleration record as that measured in the physical tests. A unique feature of this study is that a wide range of response parameters were predicted for the two nominally identical walls in which only the toe boundary condition was different. Some important lessons from this study are summarized below:

• A simple elastic-plastic soil model was shown to be sufficient to predict wall deformation, footing and reinforcement loads provided that the values of shear and bulk modulus of the backfill soil are selected accurately. Plane strain properties of the backfill sand that were back-calculated from numerical simulation of direct shear tests were required to accurately model the physical reinforced soil wall tests.

• A strain-rate independent polyester (PET) geogrid material was shown to be particularly well suited for numerical modelling and its axial stiffness properties were easily determined from conventional in-isolation constant rate-of-strain tensile tests. The in-isolation material properties were judged sufficient to model the reinforcement stiffness but the assumption of a perfect bond between the reinforcement and soil may have contributed to differences between predicted and measured loads due to reinforcement-soil slip in the 1-g physical tests at low confining pressures.

• Both physical and numerical modelling results showed that the magnitude and distribution of reinforcement connection loads during static and dynamic loading are influenced by the toe boundary condition.

• The numerically predicted zones of soil plasticity (failure wedges) increased beyond the static failure wedge (i.e. became shallower) as the input base acceleration amplitude increased. This observation is inconsistent with current North American practice that assumes the orientation of the internal failure plane for reinforcement design is described by the static load condition [α_{AE} ($k_h = k_v = 0$)]. A consequence of this deficiency is that current limit-equilibrium methods may under-estimate reinforcement anchorage lengths close to the top of the wall using pseudo-static design, which is non-conservative. Furthermore, the numerical results and measurements of mass movement at large base accelerations showed the development of a bi-linear failure mechanism which is not predicted using closed-form solutions that are variants of pseudo-static methods.

• Ground acceleration amplification based on FFT analysis was sensibly constant at about 1.1 at all locations in the numerical models. However, in the physical tests acceleration amplification varied between walls and between monitoring locations. This discrepancy warrants further investigation since an assumption in current closed-form analytical solutions for earthquake-induced reinforcement loads is that ground acceleration is constant throughout the soil backfill.

The experimental data reported from the reduced-scale model walls in this study is unique in the literature for instrumented reinforced soil walls under base excitation because a reinforcement material with scaled tensile stiffness was used together with a wide array of instrumentation including measurement of the load developed at the toe of the facing panel. The latter is necessary for verification of the matching numerical model and to quantify the important contribution of the wall facing to resist earth loads.

While there were detectable differences between physical results and numerical outcomes in many cases, the numerical simulations with simple constitutive models for the component materials were judged to have done reasonably well particularly when numerical values are compared against estimates of reinforcement load measurement accuracy. Where there was relatively poorer correspondence this may be due to low confining pressure particularly close to the top of the physical models. This is a common deficiency of reduced-scale 1-g models with frictional soils but may be less problematic if the FLAC-based model developed in this investigation is used to predict the response of full-scale walls where reinforcement confining pressures are greater. A strategy to improve reinforcement load predictions at the top of the model walls is to include an interface slip mechanism. However, the stiffness and strength of this interface is difficult to quantify from

independent laboratory testing.

In this investigation closed-form solutions gave predicted reinforcement loads that were typically within the range of estimated reinforcement loads. However, this may not be the case if nominal similar physical test walls could be carried out at prototype scale. For example, the relative influence of toe support, deformation modes and ground amplification can be expected to change with wall height. Furthermore, a very simple and aggressive accelerogram was used to excite the models in this investigation. Comparisons between numerical results and closed-form solutions should be carried out with models simulating field-scale walls and a range of actual earthquake records and possibly site-specific synthetic records before final recommendations regarding the accuracy of pseudo-static design methods are made. A verified numerical model of the type described in this paper holds promise to explore a wide range of wall response features for walls of different types, geometry, foundation stiffness and strength, material properties and seismic loading.

Acknowledgements

The writers are grateful for funding provided by the Natural Sciences and Engineering Research Council of Canada (NSERC), the Academic Research Program at RMC, grants from the Department of National Defence (Canada) and the Egyptian Government to support the research described in this paper.

References

Allen, T.M. and Bathurst, R.J. (2002), "Soil reinforcement loads in geosynthetic walls at working stress conditions", *Geosynth. Int.*, **9**(5-6), 525-566.

Allen, T.M. and Bathurst, R.J. (2006), "Design and performance of an 11-m high block-faced geogrid wall", *Proceedings of the 8th International Conference on Geosynthetics*, Yokohama, Japan, September 2006, pp. 953-956.

Allen, T.M., Bathurst, R.J. and Berg, R.R. (2002), "Global level of safety and performance of geosynthetic walls: an historical perspective", *Geosynth. Int.*, **9**(5-6), 395-450.

Allen, T.M., Bathurst, R.J., Holtz, R.D., Walters, D.L. and Lee, W.F. (2003), "A new working stress method for prediction of reinforcement loads in geosynthetic walls", *Can. Geotech. J.*, **40**(5), 976-994.

American Association of State Highway and Transportation Officials (AASHTO) (2010), *LRFD bridge design specifications*, 5th ed., AASHTO, Washington, DC, USA.

Bathurst, R.J. and Cai, Z. (1994), "In-isolation cyclic load-extension behavior of two geogrids", *Geosynth. Int.*, **1**(1), 3-17.

Bathurst, R.J. and Cai, Z. (1995), "Pseudo-static seismic analysis of geosynthetic reinforced segmental retaining walls", *Geosynth. Int.*, **2**(5), 789-832.

Bathurst, R.J. and Hatami, K. (1998), "Seismic response analysis of a geosynthetic reinforced soil retaining wall", *Geosynth. Int.*, **5**(1-2), 127-166.

Bathurst, R.J., Hatami, K. and Alfaro, M.C. (2002), *Geosynthetic reinforced soil walls and slopes: seismic aspects*, (S.K. Shukla Ed.): Geosynth. and Their Applications, Thomas Telford Ltd., London, UK, 327-392.

Bathurst, R.J., Miyata, Y., Nernheim, A. and Allen, T.M. (2008), "Refinement of K-stiffness method for geosynthetic reinforced soil walls", *Geosynth. Int.*, **15**(4), 269-295.

Bathurst, R.J., Vlachopoulos, N., Walters, D.L., Burgess, P.G. and Allen, T.M. (2006), "The influence of facing rigidity on the performance of two geosynthetic reinforced soil retaining walls", *Can. Geotech. J.*, **43**(12), 1225-1237.

Bathurst, R.J., Walters, D., Vlachopoulos, N., Burgess, P. and Allen, T.M. (2000), "Full scale testing of geosynthetic reinforced walls", Keynote paper, *ASCE Special Publication No. 103, Advances in Transportation and Geoenvironmental Systems using Geosynthetics*, *Proceedings of Geo-Denver 2000*, 5-8 August 2000, Denver, Colorado, 201-217.

Bolton, M.D. (1986), "The strength and dilatancy of sand", *Geotechnique*, **36**(1), 65-78.

Cai, Z. and Bathurst, R.J. (1995), "Seismic response analysis of geosynthetic reinforced soil segmental retaining walls by finite element method", *Comput. Geotech.*, **17**(4), 523-546.

Carotti, A. and Rimoldi, P. (1998), "A nonlinear model for the seismic response analysis of geosynthetic-reinforced soil structures", *Geosynth. Int.*, **5**(1-2), 167-201.

Chan, A.H.C. (1993), "User manual for Diana-Swandyne-II", Dept. of Civil Engineering, University of Glasgow, Glasgow, UK.

Ebling, R.M. and Morrison, E.E. (1993), "The seismic design of waterfront retaining structures", *Naval Civil Engineering Laboratory Technical Report ITL-92-11 NCEL TR-939*, Port Huenene, CA, USA, 329.

El-Emam, M.M. (2003), "Behaviour of reinforced soil walls under earthquake loading", *Ph.D. Dissertation*, Queen's University, Kingston, Ontario, Canada, 411.

El-Emam, M. and Bathurst, R.J. (2004), "Experimental design, instrumentation and interpretation of reinforced soil wall response using a shaking table", *Int. J. Phys. Model. Geotech.*, **4**(4), 13-32.

El-Emam, M. and Bathurst, R.J. (2005), "Facing contribution to seismic response of reduced-scale reinforced soil walls", *Geosynth. Int.*, **12**(5), 215-238.

El-Emam, M., Bathurst, R.J. and Hatami, K. (2004), "Numerical modeling of reinforced soil retaining walls subjected to base acceleration", *Proceedings of the 13th World Conference on Earthquake Engineering*, Vancouver, BC, 1-6 August 2004, 15.

El-Emam, M., Bathurst, R.J., Hatami, K. and Mashhour, M.M. (2001), "Shaking table and numerical modelling of reinforced soil walls", *Proceedings of the International Symposium on Earth Reinforcement*, IS Kyushu 2001, Kyushu, Japan, November 2001, Vol. 1, 329-334.

Federal Highway Administration (FHWA) (2009), *Design and construction of mechanically stabilized earth walls and reinforced soil slopes - Vols 1 and 2*, FHWA-NHI-10-024, (eds. R.R., Berg, Christopher, B.R., Samtani, N.C.), Federal Highway Administration, Washington, DC, USA.

Fujii, T., Izawa, J., Kuwano, J., Ishihara, M. and Nakane, A. (2006), "Prediction of deformation of retaining walls of geosynthetic-reinforced soil under large earthquakes", *Proceedings of the 8th International Conference on Geosynthetics*, Yokohama, Japan, September 2006, 1185-1388.

Hallquist, J.O. and Whirley, R.G. (1989), "DYNA3D user's manual: nonlinear dynamic analysis of structures in three dimensions", Rep. UCID-19592, Rev. 5, Lawrence Livermore National Laboratory, Livermore, CA, USA.

Hatami, K. and Bathurst, R.J. (2000), "Effect of structural design on fundamental frequency of reinforced-soil retaining walls", *Soil Dyn. Earthq. Eng.*, **19**, 137-157.

Hatami, K. and Bathurst, R.J. (2001), "Investigation of seismic response of reinforced soil retaining walls", *CD Proceedings of the 4th International Conference on Recent Advances in Geotechnical Earthquake Engineering and Soil Dynamics*, San Diego, CA, USA, Paper no. 7.18, 8.

Hatami, K., Bathurst, R.J. and Di Pietro, P. (2001), "Static response of reinforced soil retaining walls with non-uniform reinforcement", *Int. J. Geomech.*, **1**(4), 477-506.

Hatami, K., Bathurst, R.J. and El-Emam, M. (2005), "Acceleration amplification in the backfill of reinforced soil walls of different heights", *Proceedings of the 3rd Biot Conference on Poromechanics*, Norman, Oklahoma, USA, May 2005, (Abousleiman, Cheng & Ulm Eds.), Balkema, London, UK, 725-731.

Helwany, M.B., Budhu, M. and McCallen, D. (2001), "Seismic analysis of segmental retaining walls, I: Model verification", *J. Geotech. Geoenviron. Eng.*, **127**(9), 741-749.

Helwany, M.B. and McCallen, D. (2001), "Seismic analysis of segmental retaining walls, II: Effects of facing details", *J. Geotech. Geoenviron. Eng.*, **127**(9), 750-756.

Huang, B., Bathurst, R.J. and Hatami, K. (2009), "Numerical study of reinforced soil segmental walls using three different constitutive soil models", *J. Geotech. Geoenviron. Eng.*, **135**(10), 1486-1498.

Huang, B., Bathurst, R.J., Hatami, K. and Allen, T.M. (2010), "Influence of toe restraint on reinforced soil segmental walls", *Can. Geotech. J.*, **47**(8), 885-904.

Iai, S. (1989), "Similitude for shaking table tests on soil-structure-fluid models in 1g gravitational field", *Solids Found*., **29**(1), 105-118.
Ishihara, K. (1996), *Soil behaviour in earthquake geotechnics*, Clarendon Press, Oxford, UK, 350.
Itasca Consulting Group (2005), *Fast Lagrangian analysis of continua*, v5.0, Itasca Consulting Group, Minneapolis, MN, USA.
Koseki, J., Munaf, Y., Tatsuoka, F., Tateyama, M., Kojima, K. and Sato, T. (1998), "Shaking and tilt table tests of geosynthetic-reinforced soil and conventional-type retaining walls", *Geosynth. Int*., **5**(1-2), 73-96.
Koseki, J., Bathurst, R.J., Güler, E., Kuwano, J. and Maugeri, M. (2008), "Seismic stability of reinforced soil walls", Keynote paper, *Proceedings of the 8th International Conference on Geosynthetics, Yokohama*, Japan, 18-22 September 2006, 28.
Krishna, A.M. and Latha, G.M. (2007), "Seismic response of wrap-faced reinforced soil retaining wall models using shaking table tests", *Geosynth. Int*., **14**(6), 355-364.
Lee, K.Z.Z., Chang, N.Y. and Ko, H.Y. (2010), "Numerical simulation of geosynthetic-reinforced soil walls under seismic shaking", *Geotext. Geomembranes*, **28**(4), 317-334.
Ling, H.I. (2003), "Finite element applications to reinforced soil retaining walls–Simplistic versus sophisticated analyses", *Proceedings of Geomechanics: Testing, Modeling, and Simulation, 1st Japan–U.S. workshop on Testing, Modeling, and Simulation*, J. A. Yamamuro and J. Koseki, eds., ASCE, Reston, VA, USA, pp. 77-94.
Ling, H.I., Liu, H., Kaliakin, V.N. and Leshchinsky, D. (2004), "Analyzing dynamic behaviour of geosynthetic-reinforced soil retaining walls", *J. Eng. Mech.*, **130**(8), 911-920.
Ling, H.I., Liu, H., Kaliakin, V.N. and Mohri, Y. (2005a), "Parametric studies on the behavior of reinforced soil retaining walls under earthquake loading", *J. Eng. Mech.*, **131**(10), 1056-1065.
Ling, H.I., Mohri, Y., Leshchinsky, D., Burke, C., Matsushima, K. and Lui, H. (2005b), "Large-Scale shaking table tests on modular-block reinforced soil retaining walls", *J. Geotech. Geoenviron. Eng*., **131**(4), 465-476.
Ling, H.I., Yang, S., Leshchinsky, D., Liu, H. and Burke, C. (2010), "Finite-element simulations of full-scale modular-block reinforced soil retaining walls under earthquake loading", *J. Eng. Mech.*, **136**(5), 653-661.
Matsuo, O., Tsutsumi, T., Yokoyama, K. and Saito, Y. (1998), "Shaking table tests and analysis of geosynthetic-reinforced soil retaining walls", *Geosynth. Int*., **5**(1-2), 97-126.
Murata, O., Tateyama, M. and Tatsuoka, F. (1994), "Shaking table tests on a large geosynthetic-reinforced soil retaining wall model", *Recent Case Histories of Permanent Geosynthetic-Reinforced Soil Walls (Tatsuoka and Leshchinsky, Eds.), Proceedings of the Seiken Symposium*, Tokyo, Japan, 259-264.
National Concrete Masonry Association (NCMA) (2009), *Design manual for segmental retaining walls*, 3rd edition., M. Bernardi, ed., NCMA, Herndon, VA, USA.
Nouri, H., Fakher, A. and Jones, C.J.F.P. (2008), "Evaluating the effects of the magnitude and amplification of pseudo-static acceleration on reinforced soil slopes and walls using the limit equilibrium horizontal slices method", *Geotext. Geomembranes*, **26**(3), 263-278.
Prakash, S. (1981), *Soil dynamics*, McGraw Hill, Inc., New York, NY, USA, 426.
Rowe, R.K. and Ho, S.K. (1998), "Horizontal deformation in reinforced soil walls", *Can. Geotech. J*., **35**(2), 312-327.
Sakaguchi, M., Muramatsu, M. and Nagura, K. (1992), "A discussion on reinforced embankment structures having high earthquake resistance", *Earth Reinforcement Practice: Proceedings of the International Symposium on Earth Reinforcement Practice, IS-Kyushu '92*, Fukuoka, Kyushu, Japan, 287-292.
Seed, H.B. and Idriss, I. (1969), "Influence of soil conditions on ground motion during earthquakes", *J. Soil Mech. Found. Div. - ASCE*, **95**, 99-137.
Shinoda, M. and Bathurst, R.J. (2004), "Lateral and axial deformation of PP, HDPE and PET geogrids under tensile load", *Geotext. Geomembranes*, **22**(4), 205-222.
Tatsuoka, F., Hirakawa, D., Nojiri, M., Aizawa, H., Nishikiori, H., Soma, R., Tateyama, M. and Watanabe, K. (2009), "A new type of integral bridge comprising geosynthetic-reinforced soil walls", *Geosynth. Int*., **16**(4), 301-326.
Tatsuoka, F., Hirakawa, D., Nojiri, M., Aizawa, H., Nishikiori, H., Soma, R., Tateyama, M. and Watanabe, K. (2010), "Response to 'A new type of integral bridge comprising geosynthetic-reinforced soil wall", *Geosynth. Int*., **17**(4), 260-271.
Tatsuoka, F., Koseki, J., Tateyama, M., Munaf, Y. and Horii, K. (1998), "Seismic stability against high seismic

loads on geosynthetic-reinforced soil retaining structures", Keynote Lecture, *Proceedings of the 6th International Conference on Geosynthetics*, Atlanta, GA, USA, Vol. 1, pp. 103-142.
Vieira, C.S., Lopes, M.L. and Caldeira, L.M.M.S. (2006), "Numerical modelling of a geosynthetic reinforced soil retaining wall subjected to seismic loading", *Proceedings of the 8th International Conference on Geosynthetics*, Yokohama, Japan, September 2006, 1365-1370.
Walters, D.L., Allen, T.M. and Bathurst, R.J. (2002), "Conversion of geosynthetic strain to load using reinforcement stiffness", *Geosynth. Int.*, **9**(5-6), 483-523.
Wood, M.D. (2004), *Geotechnical modelling*, Spon Press, UK. 488.
Wood, M.D., Crewe, A. and Taylor, C. (2002), "Shaking table testing of geotechnical models", *Int. J. Physi. Model. Geomech.*, **1**(1), 1-13.
Wu, G. and Finn, L.W.D. (1996), "Seismic pressures against rigid walls", *Proceedings of the ASCE Specialty Conference on Analysis and Design of Retaining Structures against Earthquakes, Geotechnical Special Publication No. 60*, Washington, DC, USA, 1-18.
Zarnani, S. and Bathurst, R.J. (2008), "Numerical modeling of EPS seismic buffer shaking table tests", *Geotext. Geomembranes*, **26**(5), 371-383.
Zarnani, S. and Bathurst, R.J. (2009a), "Influence of constitutive model on numerical simulation of EPS seismic buffer shaking table tests", *Geotext. Geomembranes*, **27**(4), 308-312.
Zarnani, S. and Bathurst, R.J. (2009b), "Numerical parametric study of EPS geofoam seismic buffers", *Can. Geotech. J.*, **46**(3), 318-338.
Zarrabi, K. (1979), "Sliding of gravity retaining wall during earthquakes considering vertical acceleration and changing inclination of failure surface", M.Sc. Thesis, Department of Civil Engineering, Massachusetts Institute of Technology, Cambridge, MA, USA, 140.

CC